



Synthesis, structural characterization and magnetic properties of the monoclinic ordered double perovskites BaLaMSbO₆, with M = Mn, Co and Ni



M. Cecilia Blanco^a, Juan M. De Paoli^{a,1}, Sergio Ceppi^b, G. Tirao^{b,1}, Vivian M. Nassif^c, J. Guimpel^{d,1}, Raúl E. Carbonio^{a,1,*}

^a INFIQC (CONICET – Universidad Nacional de Córdoba), Departamento de Físicoquímica, Facultad de Ciencias Químicas, Universidad Nacional de Córdoba, Haya de la Torre esq, Medina Allende, Ciudad Universitaria, X5000HUA Córdoba, Argentina

^b IFEG (CONICET), Facultad de Matemáticas, Astronomía y Física, Universidad Nacional de Córdoba, Haya de la Torre esq, Medina Allende, X5000HUA Córdoba, Argentina

^c Institut Néel, CNRS et Université Joseph Fourier, BP 166, 38042 Grenoble Cedex 9, France

^d Comisión Nacional de Energía Atómica – Centro Atómico Bariloche and Instituto Balseiro, Universidad Nacional de Cuyo, Av. Bustillo 9500, 8400 Río Negro, Argentina

ARTICLE INFO

Article history:

Received 27 December 2013

Received in revised form 28 March 2014

Accepted 1 April 2014

Available online 13 April 2014

Keywords:

Double perovskites

Magnetic properties

X-ray emission spectroscopy

Neutron powder diffraction

ABSTRACT

Double perovskites BaLaMnSbO₆, BaLaCoSbO₆ and BaLaNiSbO₆, were synthesized by conventional ceramic method in air, as polycrystalline powders. The Mn and Ni compounds belong to the I 2/m monoclinic space group, while the Co perovskite belongs to the I 4/m tetragonal space group. Effective presence of Mn²⁺ has been well established by X-ray emission spectroscopy for BaLaMnSbO₆, and there is no evidence of Mn³⁺. BaLaCoSbO₆ and BaLaNiSbO₆ only show the expected 3D-antiferromagnetic behavior typical of super-superexchange interactions, while BaLaMnSbO₆ displays signs of superparamagnetism in the 40–160 K range, which arises from unbalanced antiferromagnetism inside nanoclusters formed by regions which are rich in Mn²⁺–O²⁻–Mn²⁺ paths. Neutron powder diffraction data for BaLaMnSbO₆ reveals that at 3 K, only long range order antiferromagnetic arrangement of Mn²⁺ spins on 2d octahedral sites is obtained.

© 2014 Elsevier B.V. All rights reserved.

1. Introduction

The study of double perovskites A₂BB'O₆, with a rock salt arrangement of B and B' ion has increasing interest because of their wide range of properties. For instance, they can be metallic, half-metallic, ferromagnetic or magnetoresistive, etc. [1–8]. Particularly, in the last years, interest has been renewed due to the appearance of room temperature Colossal Magnetoresistance (CMR) in A₂FeMoO₆ [1–3] and A₂FeReO₆ (A = Ca, Sr, Ba) [5–8].

If B and B' are selected in such a way that only B is paramagnetic, then magnetic properties originate on this ion, either from superexchange or super-superexchange magnetic interactions between the B ions with the rock salt arrangement. The presence of superexchange and super-superexchange paths depends of the B and B' cationic disorder on octahedral sites [9].

A wide number of AA'BB'O₆ double perovskites with A = Ca, Sr and Ba; A' = La, B = magnetic 3d transition metal ions and B' = 4th

and 5th rows closed shell transition metal ions or Sb⁵⁺, among others, have already been studied by different authors [10–14]. Most of them are highly ordered double perovskites, with predominant antiferromagnetic interactions showed by their negative Curie Weiss temperatures (θ) (normally with very low values of Neel temperatures T_N) and/or magnetic frustration as a consequence of competing interactions between ferromagnetic and antiferromagnetic order. This magnetic behavior is sensitive to the order-disorder between B and B' ions on octahedral sites.

The synthesis of new double perovskites containing M²⁺ and Sb⁵⁺ as B and B' ions using the series Mn²⁺, Co²⁺ and Ni²⁺ (with $S = 5/2$; $3/2$ and 1) are interesting since they offer the possibility to observe the effect on the magnetic behavior of the decreasing magnetic moment at the B site. Here we report, for the first time, the synthesis of these double perovskites, their structural characterization using powder X-ray diffraction (PXRD) and powder neutron diffraction (PND), their magnetic characterization using Magnetization (M) vs. Temperature and M vs. Magnetic field (H) measurements, and Mn ion oxidation state determination from X-ray emission spectroscopy (XES).

* Corresponding author. Tel.: +54 351 5353866; fax: +54 351 4334188.

E-mail address: carbonio@fcq.unc.edu.ar (R.E. Carbonio).

¹ Research Career of CONICET.

2. Materials and methods

Polycrystalline samples of BaLaMnSbO₆, BaLaCoSbO₆ and BaLaNiSbO₆ were synthesized by solid state reactions from stoichiometric quantities of high purity BaCO₃ (ACS grade), La₂O₃ (99.99%), MnO (99%), Co₃O₄ (99.9985%), Ni(NO₃)₂·6H₂O (99%), and Sb₂O₃ (99.999%). La₂O₃ was dried at 900 °C in air for 24 h prior to use. The starting materials were intimately ground, placed in alumina boats, and heated under air atmosphere in a tube furnace. In order to avoid Sb₂O₃ volatilization, the reaction mixture was first heated at 780 °C for 12 h, then at 900 °C for 10 h and finally at 1250 °C for Ni and Co perovskites and at 1350 °C for Mn perovskite, for 24 h. All heating and cooling rates were 3 deg/min.

The PXRD patterns were recorded at room temperature on a PANalytical X'Pert PRO diffractometer (in Bragg–Brentano geometry with Cu K α radiation, $\lambda = 1.5418$ Å). For the structure refinements, the PXRD data were collected in the angular range 5–120° in steps of 0.02° and with a step collection time of 10 s.

PND patterns for BaLaMnSbO₆ sample were collected at temperatures of 300 K, 100 K and 3 K in the D2B powder diffractometer at Institute Laue-Langevin (ILL), Grenoble, France, with a wavelength of 1.594 Å. The 2θ range was 8.0° up to 157.9°, with increments of 0.05°. The data collection time was approximately 3 h. PND patterns for BaLaCoSbO₆ and BaLaNiSbO₆ compounds were collected at 300 K in the D1B and D1A powder diffractometer at ILL, for wavelengths 1.28 Å for Co and 1.91 Å for Ni. The 2θ range was 10.07° up to 89.87°, with increments of 0.2° for BaLaCoSbO₆ and 8.0° up to 157.9°, with increments of 0.1° for BaLaNiSbO₆. The refinements of crystal structures from PXRD and PND data were performed by the Rietveld method [15] using the FULLPROF program [16].

High-resolution K β XES spectra of BaLaMnSbO₆ and standard manganese oxides MnO, Mn₂O₃ and MnO₂ with known oxidation states were measured using a non-conventional spectrometer [17]. The experimental data were analyzed in order to characterize the dependence of the K β' and K $\beta_{1,3}$ peaks, on the chemical environment. The measured K β emission data for BaLaMnSbO₆ was used to determine the Mn oxidation state in this compound. The high resolution K β emission spectra were recorded by scanning the analyser and the detector synchronously in steps of about 0.3 eV around the main line. With a spot size of 1.2 mm², the measured counting rate at the K $\beta_{1,3}$ line was around 90 and 1500 counts s⁻¹ for BaLaMnSbO₆ and standard Mn oxides, respectively, and the signal-to-background ratio was better than 70. The resolution of this spectrometer was determined to be 0.8 eV for the Mn-K $\beta_{1,3}$ line, for calculation details see ref [17], and the energy scale was calibrated using the value of the K $\beta_{1,3}$ line of Mn⁰⁺ given by Bearden [18] (EK $\beta_{1,3}$ = 6490.45 eV).

The magnetic measurements were performed in a commercial Quantum Design MPMS-5S superconducting quantum interference device magnetometer (SQUID) on powdered samples, in the 5–300 K temperature range and magnetic fields up to 5 T.

3. Results and discussion

3.1. Structural characterization

The room temperature PXRD patterns obtained for the three perovskites are presented in Fig. 1. All materials show good crystallinity and a high purity double perovskite phase. BaLaMnSbO₆, contains 0.74% of La₃SbO₇ (see the star marking the main peak of La₃SbO₇ in Fig. 1) and BaLaNiSbO₆, contains 2% of Ba₂LaSbO₆ (the four stars mark the main peaks of Ba₂LaSbO₆ in Fig. 1). The amount

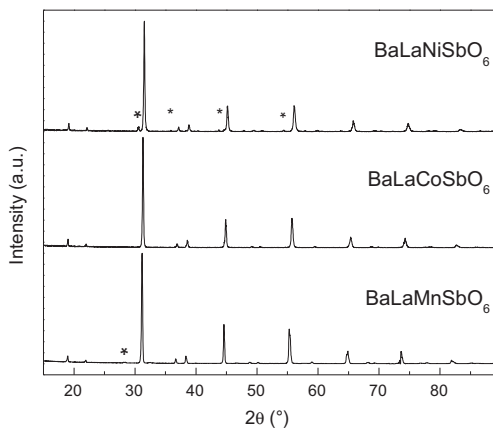


Fig. 1. Room temperature PXRD patterns for three new double perovskites. (*) correspond to the most intense impurity reflections, Ba₂LaSbO₆ for BaLaNiSbO₆ and La₃SbO₇ for BaLaMnSbO₆.

of impurity in each case was obtained from the Rietveld refinements.

Initially the three materials were well refined into the monoclinic P 2₁/n space group, commonly observed for double perovskites [10,12,14], but from systematic absences analysis, other more symmetric space groups were explored, based on the discussion presented by Faik et al. [19]. The best results for the Rietveld refinement of the room temperature PXRD and PND patterns, showed in Figs. 2 and 3, show that BaLaMnSbO₆ and BaLaNiSbO₆ belong to the monoclinic space group I 2/m, while BaLaCoSbO₆ to the tetragonal space group I 4/m. The refined parameters were: scale factor, zero shift, lattice constants, atomic positions, occupancies, pseudo Voigt parameters for the peak profile corrected by asymmetry, background and isotropic atomic displacement parameters.

Rietveld refinement of PND data was fundamental to rule out A-site ordering, because Ba²⁺ and La³⁺ ions, although having very similar X-ray scattering factors, have different neutron scattering lengths (8.3 fm for La and 5.3 fm for Ba). No superstructure peaks due to A-site ordering are present in PND data. Also, PND data allow us to refine the oxygen positions and their occupancies in the perovskite structures. For the three perovskites the refinements of the oxygen occupancies were very close to one within the uncertainty, for this reason they were fixed to unity in final refinements.

Cell parameters *a*, *b* and *c*, and cell volume, vary according to the ionic radii variation for Mn²⁺, Co²⁺ and Ni²⁺, see Table 1. At room temperature BaLaMnSbO₆ and BaLaNiSbO₆ are both monoclinic double perovskites, belonging to I 2/m space group, with *a*–*a*–*c*⁰ tilt system, according to Glazer's notation as derived by Woodward for 1:1 ordering of double perovskites [20]. The average tilting angles can be estimated as $\phi = (180 - \theta)/2$, where $\theta = \langle B-O-B' \rangle$. BaLaCoSbO₆ is a tetragonal double perovskite, in space group I 4/m, with *a*⁰*a*⁰*c* tilt system.

BaLaMnSbO₆, retains the monoclinic I 2/m symmetry at 100 K, but there is a monoclinic I 2/m to monoclinic P 2₁/n structural transition at lower temperatures due to modification of the tilt angles, produced as a consequence of the long range ordering of the magnetic moments, as will be explained later. This transition involves the incorporation of a new in-phase tilt around *c* axis, and, consequently, the tilt system, at 3 K, is *a*–*a*–*c*⁺, for the double perovskite. The cell parameters obtained for all temperatures are shown in Table 1. There is a small decrease in volume (1.4%) from room temperature to 3 K.

Structural parameters for the three phases at room temperature are displayed in Table 2 and main bond distances and angles are listed in Table 3. From M²⁺/Sb⁵⁺ ion occupancies, listed in Table 2, it is possible to observe the very low B antisite disorder for the members of this family, being 6% for both BaLaMnSbO₆ and BaLaNiSbO₆, and 1% for BaLaCoSbO₆. We must remark that isotropic temperature factors for some oxygens are quite low for BaLaMnSbO₆ at 100 (O1) and 3 K (O3). This low *B*_{iso} values for oxygens were found for other double perovskites containing Sb [21–23]. We assigned these low values to the strong covalent bond Sb–O. Calculations made by Larréola et al. [24], showed that in Pb₂ScSbO₆ there is a clear indication of strong electron density in the bonds Sb–O, indicating strong covalency.

The $\langle B-O \rangle$ average distances, in Table 3, decrease in the sequence Mn²⁺ > Co²⁺ > Ni²⁺ according to the different ionic radii of the M²⁺ magnetic ions (Mn²⁺(HS) = 0.97 Å; Co²⁺(HS) = 0.885 Å; Ni²⁺ = 0.83 Å). The $\langle B'-O \rangle$ average distance is shorter than any of the $\langle B-O \rangle$ average distances which is in agreement with the smaller ionic radii for diamagnetic Sb⁵⁺ (0.74 Å). Tilt angles are smaller than 8° at room temperature for all materials.

Only PND data taken at 3 K for the double perovskite BaLaMnSbO₆ presents signs of long range magnetic order (showed in Fig. 4, left side). The corresponding magnetic phase was added to

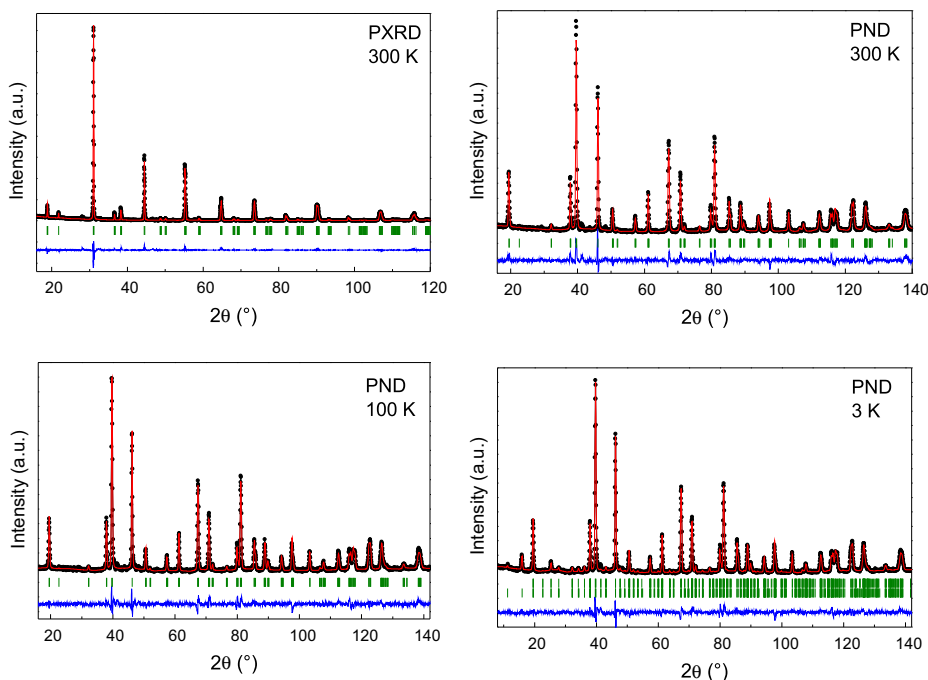


Fig. 2. Observed (dots), calculated (full line) and difference (bottom line) for PXRD and PND patterns after the refinement of the crystal structure of BaLaMnSbO₆ at RT in upper panel and for PND patterns at 100 and 3 K in lower panel. The series of tick marks correspond to the Bragg reflections of the main perovskite phase in all cases, but in 3 K PND pattern the bottom series correspond to the low temperature magnetic phase.

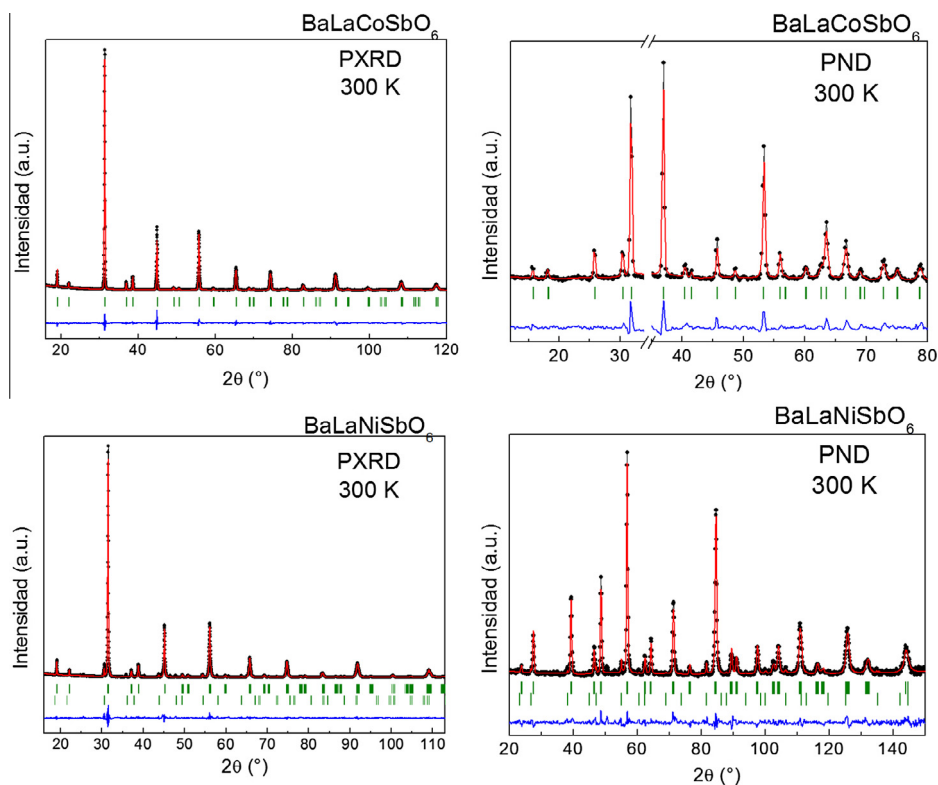


Fig. 3. Observed (dots), calculated (full line) and difference (bottom line) for PXRD and PND patterns after the refinement of the crystal structure of BaLaCoSbO₆ at RT in upper panel and for BaLaNiSbO₆ in lower panel. The series of tick marks correspond to the Bragg reflections of the main perovskite phase in all cases. In BaLaNiSbO₆ the second series correspond to the minority phase Ba₂LaSbO₆ (2%).

the crystallographic Rietveld refinement of PND data, and the magnetic reflections were refined by an antiferromagnetic arrangement of Mn²⁺ ions. Attempts to assign a magnetic cell in the

same space group used for the higher temperatures, I 2/m, were unsuccessful. A good refinement of the antiferromagnetic cell was only obtained when monoclinic P 2₁/n space group was

Table 1

Refined cell parameters and discrepancy factors after the Rietveld refinement from PND data taken at 300, 100 and 3 K for BaLaMnSbO₆ and at 300 K for BaLaCoSbO₆ and BaLaNiSbO₆.

M	BaLaMnSbO ₆			BaLaCoSbO ₆	BaLaNiSbO ₆
	300	100	3	300	300
T (K)	300	100	3	300	300
SG	I 2/m	I 2/m	P 2 ₁ /n	I 4/m	I 2/m
a (Å)	5.7508(5)	5.7285(4)	5.7264(3)	5.707(3)	5.6686(4)
b (Å)	5.7638(4)	5.7387(3)	5.7378(3)	5.707(3)	5.6907(3)
c (Å)	8.1422(7)	8.1045(5)	8.1035(5)	8.062(6)	8.0159(5)
β (°)	90.244(1)	90.277(1)	90.279(1)	90.000	89.924(1)
V (Å ³)	269.88(4)	266.43(3)	266.25(3)	262.5(3)	258.58(3)
χ ²	5.17	3.47	4.05	3.23	4.06
λ (Å)	1.594	1.594	1.594	1.280	1.910
R _{wp}	17.8	17.2	17.1	13.3	18.8
R _p	15.5	20.3	20.6	16.8	13.5
R _{Bragg}	7.09	5.97	7.14	4.40	5.13

considered for this temperature. Rietveld refinement of 3 K PND data using an antiferromagnetic cell, with $k = 0$, are shown in Fig. 4, upper inset, left side. The refined magnetic cell with magnetic moments corresponding to 2d crystallographic site mainly occupied by Mn²⁺, is shown in Fig. 4, right side. Magnetic moments corresponding to the small amount (6%) of Mn²⁺ present in 2c site remains essentially disordered. The refined net ordered magnetic moment for collinear antiferromagnetic alignment is 2.58(5) μ_B, being less than half the theoretical one for Mn²⁺. This might be indicating that there is a large degree of frustration in this material.

Fig. 5, left and right panels, illustrates the 2D-representations of the arrangement of M²⁺ and Sb⁵⁺ ions over the octahedral sites for the 1% and the 6% disorder cases. These 2D-statistical arrangements highlight the appearance of M²⁺ rich areas randomly distributed over the bulk material. Such areas are enclosed by circles in

this simplified 2D model but can be visualized as 3D-nanoclusters, where only M²⁺–O^{2–}–M²⁺ superexchange paths are present. Moreover, superexchange paths in most cases contain uncompensated antiparallel spins, i.e., there are more spins up than spins down or vice versa. The larger the cationic disorder degree, the more frequent the presence of such 3D-nanoclusters. This is similar to the model used in A₃B₂B'O₉ perovskites to explain the large T_C values obtained for this stoichiometry compared to the A₂BB'O₆ stoichiometry [25,26]. The main difference is that the A₃B₂B'O₉ has a large “intrinsic” antisite disorder [27], while in A₂BB'O₆ stoichiometry antisite disorder is usually low or nonexistent.

3.2. X-ray emission spectroscopy (XES): Mn oxidation state

With the aim to determine the Mn oxidation state we measured XES. Each high-resolution Kβ emission spectrum was normalized to the incident intensity in order to take into account beam fluctuations. To calculate the spectral parameters, the spectra were first normalized to a constant value for the maximum of Kβ_{1,3} line. Then, three Voigt functions, representing the K', Kx and K_{1,3} peaks, and the Exponentially Modified Gaussian function, to include KMM radiative Auger effect (RAE) [28,29], were adjusted in order to reproduce the peaks features. Also a linear background was subtracted. The energy position of the RAE peak was determined from the atomic energy of the M_{VI,III} level [30]. The experimental resolution was characterized by the Gaussian width. The experimental errors of the spectral parameters were determined from the fitting uncertainties.

The Kβ' feature presents a broad peak at the low energy side of the main Kβ_{1,3} line which becomes more noticeable for low oxidation states, see Fig. 6, left side. The energy of the Kβ' satellite line relative to the main Kβ_{1,3} line decreases linearly with the oxidation

Table 2

Positional and thermal parameters, and occupancies for BaLaMnSbO₆, BaLaCoSbO₆ and BaLaNiSbO₆, after the Rietveld refinement from PND data. Since the maximum multiplicity in each space group in this table has a different value, we normalize Occ., to 1 for all cases in order to compare them.

T (K)	Ion	Wyckoff site	x	y	z	B _{iso}	Occ.
300	BaLaMnSbO ₆ (SG: I 2/m (#12))						
	Ba/La	4i	0.4959(1)	0	0.2526(1)	0.606(2)	0.5/0.5
	Mn/Sb(1)	2d	0	0	1/2	0.418(1)	0.944(2)/0.056(2)
	Mn/Sb(2)	2a	0	0	0	0.198(2)	0.056(2)/0.944(2)
	O1	4i	−0.0380(2)	0	0.2471(1)	1.66(2)	1
	O2	8j	0.2255(1)	0.2486(2)	0.0328(1)	1.91(1)	1
100	I 2/m (#12)						
	Ba/La	4i	0.4902(2)	0	0.2529(1)	0.83(1)	0.5/0.5
	Mn/Sb(1)	2d	0	0	1/2	1.16(5)	0.944(2)/0.056(2)
	Mn/Sb(2)	2a	0	0	0	0.70(2)	0.056(2)/0.944(2)
	O1	4i	−0.0376(1)	0	0.2501(1)	0.25(1)	1
	O2	8j	0.2246(1)	0.2427(2)	0.0354(1)	1.99(1)	1
3	P 2 ₁ /n (#14)						
	Ba/La	4e	0.0107(2)	0.0008(2)	0.2459(1)	0.76(1)	0.5/0.5
	Mn/Sb(1)	2d	1/2	0	0	1.18(5)	0.944(2)/0.056(2)
	Mn/Sb(2)	2c	1/2	0	1/2	0.62(3)	0.056(2)/0.944(2)
	O1	4e	0.2347(2)	0.2709(2)	0.0306(2)	1.75(3)	1
	O2	4e	0.2145(2)	−0.2451(2)	0.0398(2)	2.04(3)	1
O3	4e	−0.0377(1)	0.5041(2)	0.2506(1)	0.17(1)	1	
300	BaLaCoSbO ₆ (I 4/m (#87))						
	Ba/La	4d	0	1/2	1/4	0.45(2)	0.5/0.5
	Co/Sb(1)	2a	0	0	0	0.17(4)	0.984(2)/0.016(2)
	Co/Sb(2)	2b	0	0	1/2	0.12(1)	0.016(2)/0.984(2)
	O1	4e	0	0	0.254(3)	0.90(3)	1
	O2	8h	0.288(1)	0.222(2)	0	2.7(1)	1
300	BaLaNiSbO ₆ (I 2/m (#12))						
	Ba/La	4i	0.5094(1)	0	0.2493(1)	0.445(4)	0.5/0.5
	Ni/Sb(1)	2d	0	0	1/2	0.10(2)	0.940(4)/0.060(4)
	Ni/Sb(2)	2a	0	0	0	0.18(1)	0.060(4)/0.940(4)
	O1	4i	−0.0171(6)	0	0.2505(1)	1.11(5)	1
	O2	8j	0.2515(4)	0.2391(4)	0.0320(2)	1.33(2)	1

Table 3Main distances, angles and tilt angles (δ) after Rietveld refinement of PND data for BaLaMnSbO₆, BaLaCoSbO₆ and BaLaNiSbO₆.

T (K)	BaLaMnSbO ₆			BaLaCoSbO ₆	BaLaNiSbO ₆
	300	100	3	300	300
<i>Distances (Å)</i>					
B–O1	2.070(1) × 2	2.035(1) × 2	2.0315(1) × 2	2.05(2) × 2	2.002(4) × 2
B–O2	2.160(1) × 4	2.181(1) × 4	2.1816(1) × 2	2.076(8) × 4	2.062(2) × 4
B–O3			2.1884(1) × 2		
⟨B–O⟩	2.130	2.132	2.134	2.07	2.042
B'–O1	2.024(1) × 2	2.040(1) × 2	2.0435(1) × 2	1.98(2) × 2	2.010(4) × 2
B'–O2	1.950(1) × 4	1.917(1) × 4	1.9362(1) × 2	1.994(8) × 4	1.988(2) × 4
B'–O3			1.8954(1) × 2		
⟨B'–O⟩	1.975	1.958	1.958	1.99	1.995
<i>Angles (°)</i>					
B–O1–B'	167.8(1)	167.9(1)	167.7(1)	180.0(1)	174.5(2)
B–O2–B'	164.1(1)	163.3(1)	159.6(1)	165.1(3)	165.2(1)
B–O3–B'			165.9(1)		
δ	6.1	6.1	6.2	0.0	2.8
δ	8.0	8.4	10.2	7.5	7.4
δ	0.0	0.0	7.1	0.0	0.0

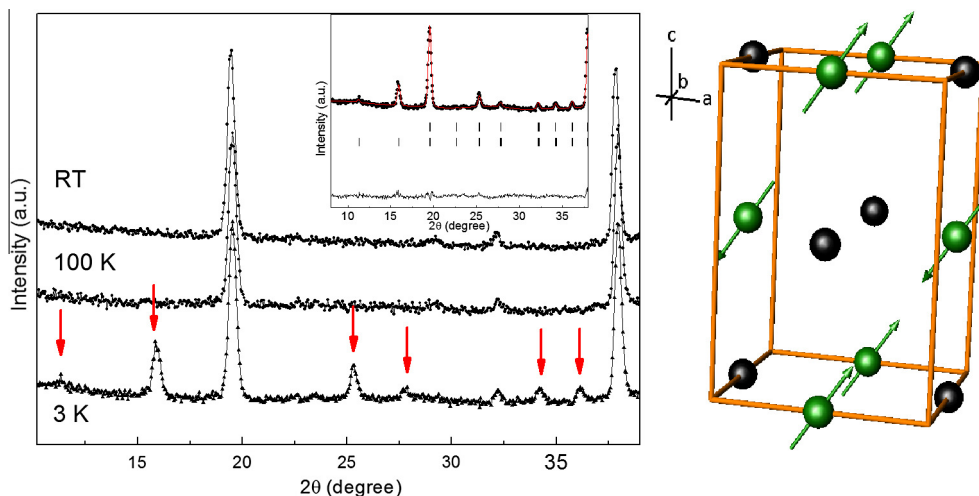


Fig. 4. BaLaMnSbO₆: left side, PND data at 3, 100 and 300 K, arrows correspond to long range magnetic order reflections at 3 K. Inset: low angle view for Rietveld refinement including both, crystallographic and magnetic phases. Right side: Magnetic cell for 3 K PND data, Ba²⁺, La³⁺ and O²⁻ ions omitted, 2d sites ions (mainly Mn²⁺) with arrows representing antiferromagnetic arrangement, 2c sites ions (mainly Sb³⁺) represented by black spheres (without arrows).

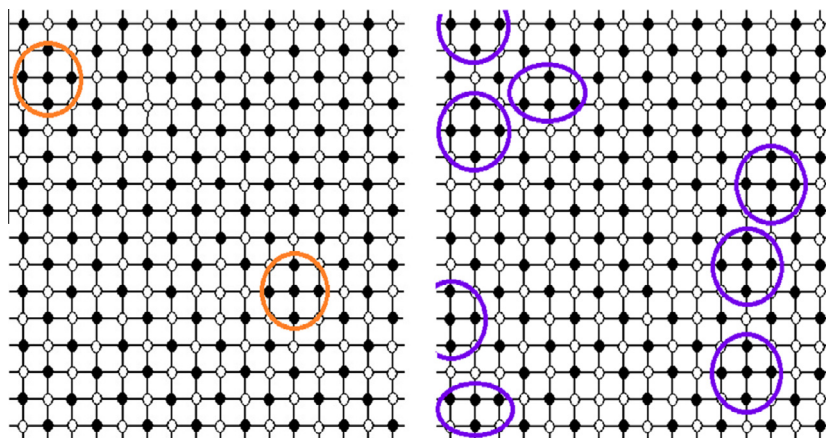


Fig. 5. Full view for 2D-statistical distribution of M²⁺ (full circles) and Sb³⁺ (empty circles) ions over octahedral sites. Left side: BaLaCoSbO₆ (1% disorder), right side: BaLaMnSbO₆ and BaLaNiSbO₆ (6% disorder). Major circles enclose M²⁺ ions rich areas. Ba²⁺, La³⁺ and O²⁻ ions were omitted for better understanding.

state in agreement with results reported by other authors [31–34]. The intensity of the Kβ' line (I-Kβ') relative to the total intensity of the main Kβ region (including the Kβ' and Kβ_{1,3} lines, whose

intensity per Mn must be chemically invariant [26]), decreases as the oxidation state increases, (Fig. 6, right side). The same linear trend was also seen by other authors [32,34,35]. Using this features

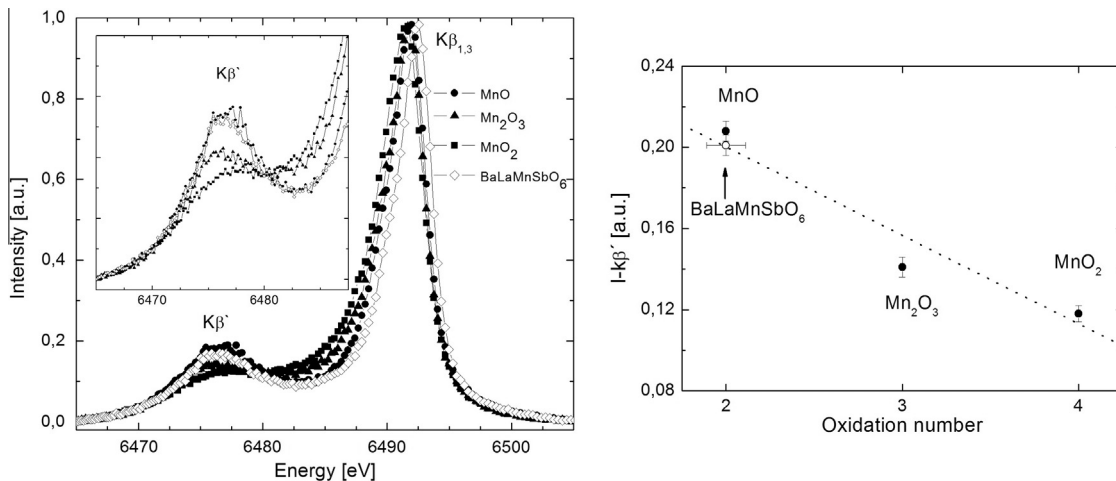


Fig. 6. Left side: satellite lines of the Mn-K β emission spectra for Mn compounds. The K β' satellite line and the main K $\beta_{1,3}$ are indicated. Inset: Region of K β' satellite line in detail. Right side: intensity of the K β' line ($I\text{-K}\beta'$) relative to the total intensity of the main K β region, as a function of oxidation states. (●): experimental data for known binary Mn oxides. (○): experimental data for BaLaMnSbO₆. (---): linear fit for all Mn oxides.

of the $I\text{-K}\beta'$ line, the oxidation state of Mn in BaLaMnSbO₆ can be calculated by means of a linear regression, resulting in a value of (2.0 ± 0.1) .

3.3. Magnetic properties

The thermal evolution of the magnetic susceptibility (χ) at 50 kOe for the three compounds is shown in Fig. 7, left panel. χ decreases in the sequence Mn²⁺ ($S = 5/2$) \rightarrow Co²⁺ ($S = 3/2$) \rightarrow Ni²⁺ ($S = 1$), which is in agreement with the S values of the HS ions.

If BaLaMnSbO₆ magnetic measurements are independently considered, in Fig. 7, central and right panels, the behavior is complex. For an applied field of 0.5 kOe, the susceptibility exhibits a rise below 200 K, and displays a cusp at around 14 K. When the applied field increases, the susceptibility rise becomes less sharp, but the cusp is still substantial at 5.0 kOe. When the applied field is about 50.0 kOe, the cusp disappears as evidence of possible weak spin-glass behavior as observed by Mandal et al. for monoclinic P 2₁/n SrLaMnSbO₆ [12]. At low field strengths, the magnetization shows significant irreversibility between the FC and ZFC data. These differences vanish at higher fields. The inverse of the susceptibility departs from the lineal behavior below 250 K.

Both BaLaCoSbO₆ and BaLaNiSbO₆ display 3-dimensional anti-ferromagnetic behavior at the studied fields, and the inverse susceptibilities are linear in the range 150–300 K. From the maximum in the χ vs. T curves it is possible to determine T_N , see Fig. 8. The values are listed in Table 4. BaLaNiSbO₆ shows some irreversibility between FC and ZFC curves below T_N at applied fields of 10.0 kOe.

All data were well fitted with a Curie–Weiss law, in the 250–300 K range for BaLaMnSbO₆ and in the 150–300 K range for BaLaCoSbO₆ and BaLaNiSbO₆. Even though when a temperature dependent paramagnetic contribution (χ_{TIP}), was considered in the fits, this was successfully adjusted only for BaLaNiSbO₆.

From the data in Table 4 it is possible to conclude that there are substantial differences between BaLaMnSbO₆ and the other compounds. The obtained values for Weiss temperatures (θ) for BaLaMnSbO₆, positive for all measured fields, point to the presence of predominant ferromagnetic correlations, while the negative θ values for BaLaCoSbO₆ and BaLaNiSbO₆, indicate the expected antiferromagnetic correlations for both Co²⁺–O–Sb⁵⁺–O–Co²⁺ and Ni²⁺–O–Sb⁵⁺–O–Ni²⁺ paths in agreement with Goodenough–Kanamori rules for $d^7\text{-}d^7$ and $d^8\text{-}d^8$ double superexchange paths. For BaLaMnSbO₆, from the first derivative, dM/dT , for applied fields of 0.5

and 5.0 kOe the ferromagnetic transition temperatures can be determined as $T_C \approx 160$ K, but this transition temperature could not be established for BaLaCoSbO₆ and BaLaNiSbO₆.

Regarding the BaLaMnSbO₆ perovskite, the possible presence of any magnetic impurities, particularly the expected ferromagnetic or antiferromagnetic ones like (La, Ba)MnO₃ and MnO, can be ruled out since there are no signs of the presence of such impurities neither in PXRD nor in PND patterns. Moreover perovskites like La_{1-x}Ba_xMnO₃ [36] have T_C in the 184–228 K temperature range, and contain a combination of Mn³⁺ and Mn⁴⁺. Previously presented results of XES do not shows any sign of the presence of such oxidation states for Mn ions.

Besides, considering other Mn²⁺ containing perovskites, similar magnetic properties have been found. In the work by Mandal et al. [12] on the LaSrMnSbO₆ double perovskite, the magnetic behavior and the nonlinear magnetization below 300 K was indicative of the presence of FM clusters, which did not originate magnetic long range order, according to low temperature PND data. Recent results by Franco et al. [37] on LaPbMnSbO₆, show a P 2₁/n space group, no detectable crystallographic antisite disorder, and an unexpected magnetic order at 45 K, which is explained based on ferrimagnetic ordering of isolated disordered regions.

For BaLaMnSbO₆ the effective paramagnetic moments (μ_{eff}) are around 5 μ_B and are a little lower than 5.92 μ_B , the spin only theoretical value corresponding to Mn²⁺ (HS) ($t_{2g}^3 e_g^2$, $S = 5/2$). For BaLaCoSbO₆ we obtained μ_{eff} between 5.07 and 5.19 μ_B which are higher than the theoretical spin only paramagnetic moment for Co²⁺ (HS) ($t_{2g}^5 e_g^2$, $S = 3/2$, $\mu_{\text{eff}} = 3.87 \mu_B$), indicating some orbital contribution to the paramagnetic moment. Co²⁺ (HS) in octahedral environment frequently shows unquenched orbital contribution with experimental values of μ_{eff} around 5.2 μ_B [10,11], close to the total unquenched theoretical paramagnetic moment for Co²⁺ which is 6.63 μ_B . Finally, the effective paramagnetic moments for BaLaNiSbO₆ are near the theoretical spin only paramagnetic moment of 2.83 μ_B , corresponding to Ni²⁺ ($t_{2g}^6 e_g^2$, $S = 1$).

Double perovskites favor geometric frustration due to the interpenetrating B and B' fcc rock salt magnetic sublattices based on edge-shared tetrahedral network. Frustration factors are calculated as $f = |\theta|/T_N$ and are usually <3 , for unfrustrated cubic antiferromagnets [38] and >10 for strongly frustrated materials. In our case we have intermediate values, see Table 4. The lowest values are found for the Ni compound. The Co and Mn compounds have similar values to those reported for LaACoNbO₆ (A = Ca, Sr, and Ba) [10].

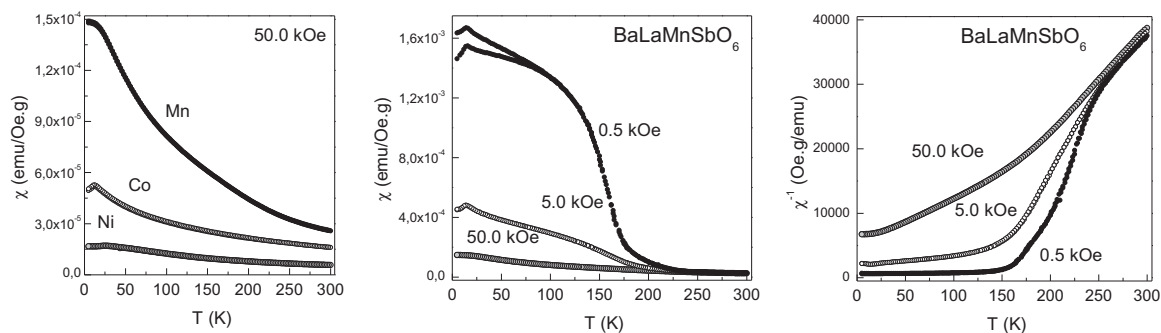


Fig. 7. Left panel: magnetic susceptibility (χ) vs. temperature at 50.0 kOe for BaLaMnSbO₆ (M = Mn, Co or Ni) under both ZFC and FC conditions. Central panel: χ vs. T at several applied fields for BaLaMnSbO₆. Right panel: χ^{-1} vs. T for BaLaMnSbO₆.

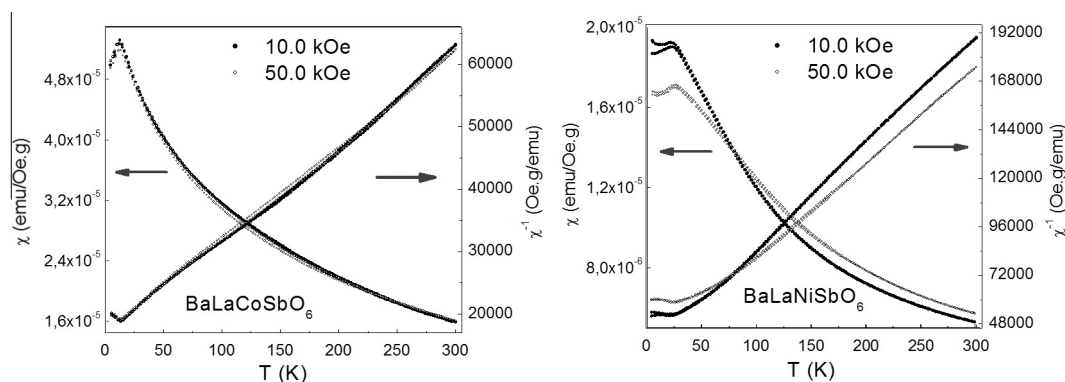


Fig. 8. χ vs. T and χ^{-1} vs. T at two applied fields in ZFC and FC conditions, for BaLaCoSbO₆, left panel, and for BaLaNiSbO₆, right panel.

Table 4

Magnetic parameters obtained according Curie–Weiss law fitting of data, from Figs. 7 and 8, in paramagnetic region. Curie constant: C , Weiss temperature: θ , paramagnetic effective moment: μ_{eff} . Ferromagnetic transition temperature, T_C , obtained as dM/dT , Neel temperature, T_N , obtained from susceptibility top, and, Frustration factor, f , calculated according $|\theta|/T_N$.

H (kOe)	C (emu K/Oe g)	θ (K)	μ_{eff} (μ_B/Mn^{2+})	T_C (K)	T_N (K)	$f = \theta /T_N$
<i>BaLaMnSbO₆</i>						
0.5 – ZFC	0.0059	79.81	5.07	164.0	14.1	5.66
0.5 – FC	0.0059	77.41	5.09			5.49
5 – ZFC	0.0056	85.14	4.96	160.0	14.1	6.03
5 – FC	0.0056	85.14	4.96			6.03
50 – ZFC	0.0061	62.35	5.19	–	–	–
50 – FC	0.0060	64.44	5.15			–
<i>BaLaCoSbO₆</i>						
10 – ZFC	0.0056	–50.7	4.95	–	12.4	4.1
10 – FC	0.0059	–69.8	5.09			5.6
50 – ZFC	0.0061	–80.0	5.19	–	12.4	6.5
50 – FC	0.0063	–89.0	5.27			7.2
<i>BaLaNiSbO₆</i>						
10 – ZFC	0.0015	–34.0	2.58	–	χ_{TIP} (emu/Oe.g) = 7×10^{-7} 23.5	1.5
10 – FC	0.0015	–30.6	2.58			1.3
50 – ZFC	0.0017	–34.4	2.74	–	26.5	1.3
50 – FC	0.0018	–44.2	2.82			1.7

The evolution of M vs. H in BaLaMnSbO₆ at 40 K and 5 K is displayed in the inset of Fig. 9, left panel. The data show some type of ferromagnetic behavior without hysteresis at low fields for both temperatures superimposed to a linear antiferromagnetic or paramagnetic contribution. This nonlinear behavior without hysteresis is consistent with the possibility of some superparamagnetic behavior [39]. Since from PND data at 100 and 3 K, see Fig. 2, there is no evidence of magnetic impurities, we propose below a microscopic mechanism for this possible superparamagnetism.

Saturation magnetizations, obtained after subtracting linear antiferromagnetic contribution are 0.26 μ_B/mol at 5 K and 0.20 μ_B/mol at 40 K, see Fig. 9, left panel. These values are around 5% of the expected 5 μ_B/mol for an ideal ferromagnetic behavior. This behavior after subtracting the linear contribution is very similar to the one observed for some manganite perovskites with ferromagnetic clusters that show a Brillouin function dependence [39–44]. According to this, the ferromagnetic like component observed in the M vs. H data for the double perovskite BaLaMnSbO₆,

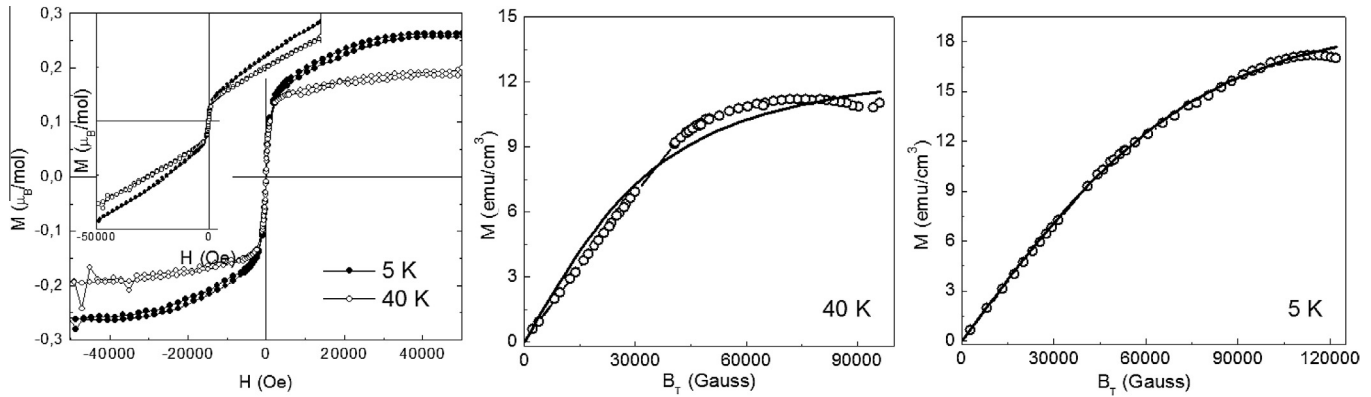


Fig. 9. Left panel: magnetization vs. magnetic field at 40 and 5 K, after linear subtraction. Inset: data not corrected. Central and right panels show the Brillouin function fit of magnetization data vs. induced field (B_T) at 40 and 5 K. Circles: experimental data, solid line: Brillouin function fitting.

can be taken as the manifestation of small clusters with uncompensated antiferromagnetic interactions $Mn^{2+}-O^{2-}-Mn^{2+}$ which come from the 6% B-site cationic disorder, see Fig. 5, right panel. Similar behavior has been reported by Mandal et al. for monoclinic $P2_1/n$ $SrLaMnSbO_6$ double perovskite [12], although in that case the ferromagnetism was assigned to Zener double exchange due to the presence of Mn^{3+} , which is not present in our compound. They also associated the observed ferromagnetism to ferromagnetic clusters originated in the presence of B site disorder. Moreover they attributed the low magnitude of the non-linear rise of the magnetization vs. H curve without any hysteresis to a superparamagnetic-like behavior. Mandal et al. [22] found for Sr_2MnSbO_6 that M vs H data showed at 50 K Brillouin-like curvature with no hysteresis and also attributed this to ferromagnetic coupled clusters, although in this case Mn is in the 3+ oxidation state.

In order to investigate the possible Brillouin-like behavior in $LaBaMnSbO_6$, we fit a Brillouin function to the M vs. H data to determine the effective spin contribution of the nanoclusters to the ferromagnetism. The field dependence of the magnetization at 5 and 40 K, after subtracting the linear contribution, were adjusted to the relation: $M = M_S B_S$, where

$$B_S(x) = (1/S)[(S + 1/2)\coth x(S + 1/2) - (1/2)\coth(x/2)]$$

with, $M_S = ng\mu_B S$, $x = g\mu_B B/kT$, and $B = H + 4\pi M + \lambda M$; which is the induced field and contains the Weiss molecular field constant for ferromagnetic interaction (λ). This constant was obtained from the ferromagnetic transition constant, T_C , and Curie constant, C , as: $T_C = \lambda C/\mu_0$ for both temperatures, M_S and the effective spin value, S_{eff} were obtained from the fit. We define $x = aB$, with: $a = g\mu_B/kT$, and $g = 2$.

From the obtained S_{eff} value and the expected spin quantum number S_{theo} for Mn^{2+} (HS), the spin-canting angle was estimated using the relation:

$$\beta = \cos^{-1}(S_{eff}/S_{theo})$$

The fits are shown in central and right panels of Fig. 9 together with the parameters in Table 5. A lower value of S_{eff} compared with the theoretical value of $2.5 \mu_B$ is obtained at 5 K, the β value of 80.0° suggest an arrangement of spins close to an almost perpendicular canting between neighboring magnetic ions into the small clusters, resulting in a very small ferromagnetic contribution, not superparamagnetic in nature at all. The nanoclusters, even magnetically ordered below 160 K, are not numerous enough to display a long range magnetic order in low temperature PND data, and consequently the refinements contain only the antiferromagnetic cell.

Table 5

Parameters obtained from Brillouin function fitting. M_S and S_{eff} are the saturated magnetic moment and the effective spin quantum number.

T (K)	a Factor	M_S (emu/cm ³)	S_{eff}	Angle β ($^\circ$)	S_{theo}
5	3.36×10^{-6}	19.25	0.433	80.02*	5/2
40	2.68×10^{-5}	13.44	18.73	20.53**	(5/2)8

Both * and ** calculated according $\cos^{-1}(S_{eff}/S_{theo})$, particular considerations exposed in text.

At 40 K the observed situation is quite different; the obtained S_{eff} value is much bigger, indicating a possible superparamagnetic contribution to the whole magnetic behavior at such temperature. For the estimation of the corresponding canting angle it was necessary to propose a number of magnetic ions that constitute the nanocluster. Let's assume that as a mean value such number is 8, since in this way the theoretical S_{theo} value gives $S_{theo} = 8(5/2) = 20$, very close to the experimental value (18.73). Then, the canting angle can be calculated according to the previous expression.

The obtained value is about 20° . This superparamagnetic contribution present at 40 K is not the same in nature than the residual ferromagnetic-like behavior established at lower temperatures. We propose that below T_N , the bulk antiferromagnetic arrangement surpass the superparamagnetic contribution coming from the small clusters. This change of magnetic regime becomes clear from the contrast between the extremely low S_{eff} value obtained at 5 K and the noticeable higher S_{eff} value at 40 K. The first can be interpreted as a small fraction of ions having the theoretical spin quantum number $S_{theo} = 5/2$, at 5 K. The second is compatible with a collective magnetic moment $S_{theo} = 8(5/2) = 20$, at 40 K.

At the top of Fig. 10 we show the suggested magnetic behavior for three stages. On the right panel, certain alignment of nanoclusters with net magnetic moments exists below and near T_C . This alignment of nanoclusters with the applied field occurs in a ferromagnetic arrangement, but there is no evidence of interactions between neighboring clusters, which is coherent with superparamagnetism. On the central panel, below T_C and near T_N , the alignment of clusters with net magnetic moments remains but the antiferromagnetic arrangement of bulk material has already started (the illustration is an oversimplified picture). At the left panel, below T_N , the net magnetic component of the clusters has been erased by the final 3D antiferromagnetic arrangement of the material. It just remains a small quantity of nanoclusters with the spins almost perpendicular to the neighboring ions, which is the responsible for the remaining short range ferromagnetic-like behavior at 5 K.

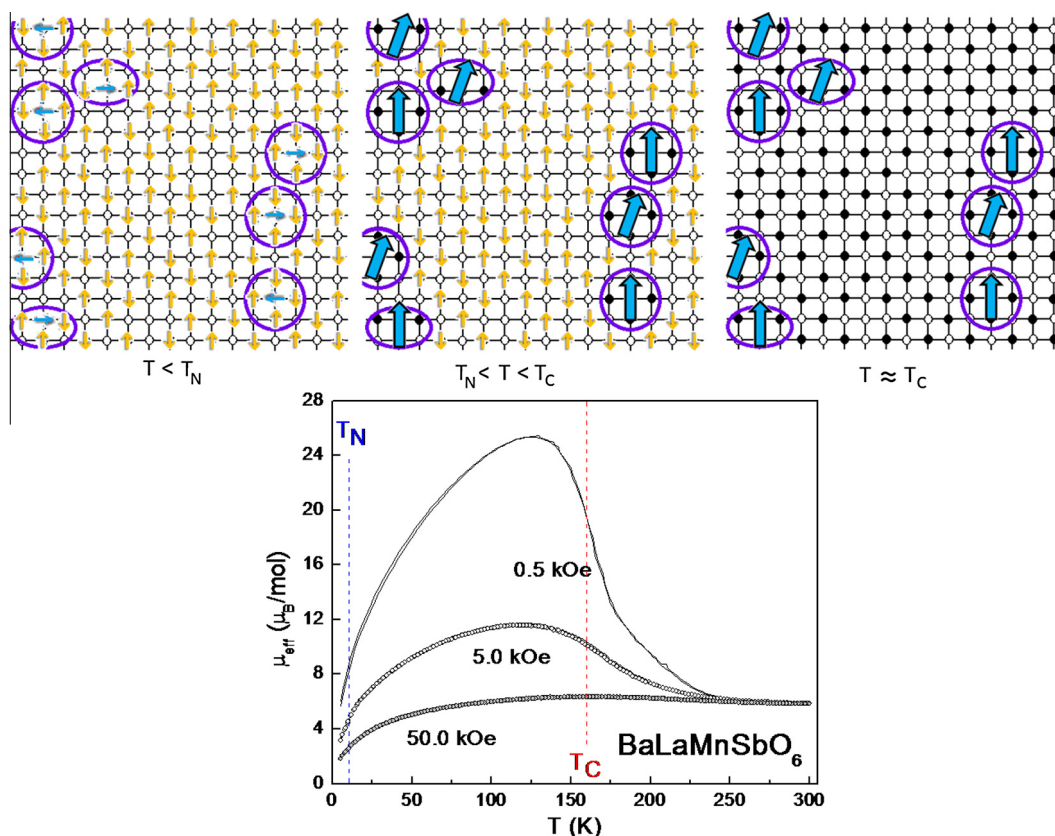


Fig. 10. Upper panel: oversimplified description for magnetic behavior as a function of temperature. Right side: nanoclusters formation and superparamagnetic behavior at T around T_C . Central panel: partial antiferromagnetic order of bulk material coexisting with superparamagnetic regions, near T_N . Left side: long range 3D antiferromagnetic arrangement and almost perpendicular magnetic components remaining from short range arrangement of neighbor spins for $T < T_N$. Lower panel: plots of effective moment μ_{eff} vs. T , deduced from χT vs. T data at three studied fields. Dashed lines correspond to T_C (red) and T_N (blue). (For interpretation of the references to color in this figure legend, the reader is referred to the web version of this article.)

Bottom of Fig. 10 illustrates μ_{eff} as function of T for BaLaMnSbO₆ at the three H values, with dashed lines indicating, T_C and T_N . The proposed superparamagnetism is observed between these two order temperatures. An extra feature is the field dependence of this behavior, because at an applied field of 50.0 kOe the material becomes only antiferromagnetic. The ferromagnetic like contribution, as can be seen in left side of Fig. 9, is present only at quite low applied fields. From Brillouin function fit to the M vs. H data at 40 K, the effective magnetic moment reaches a value of around 19 μ_B/mol , see Table 5, in agreement with the measured value of around 10–20 μ_B/mol at 0.5 kOe, on bottom of Fig. 10.

The described model is not able to differentiate if the ferromagnetic component comes from weak ferromagnetism, from spin canting, or even if it is the manifestation of only unbalanced antiferromagnetism. We assume that spin canting between adjacent magnetic ions is a really interesting possibility, but has not been observed between two nearest neighbor Mn²⁺, when the angles in Mn²⁺–O–Mn²⁺ paths are near 180°. According with Goodenough–Kanamori rules for both, d^5 – d^5 superexchange and double superexchange paths, the most frequent Mn²⁺–O–Sb⁵⁺–O–Mn²⁺ paths, at almost 180° angles, are antiferromagnetic while the really infrequent Mn²⁺–O–Mn²⁺ paths should be antiferromagnetic too. Consequently, it is probable that unbalanced antiferromagnetism is the ultimate reason for the magnetic component of clusters.

With the same disorder degree and consequently, the same amount of nanoclusters with predominant Ni²⁺–O²⁻–Ni²⁺, but being Ni²⁺ ($S = 1$), an ion with small magnetic moment, the behavior of BaLaNiSbO₆ is only antiferromagnetic. There are no signals of a complex magnetic behavior at the studied fields.

4. Conclusions

Double perovskites BaLaMnSbO₆, BaLaCoSbO₆ and BaLaNiSbO₆, have been synthesized by conventional ceramic method in air atmosphere, as polycrystalline powders. The Mn and Ni compounds belong to $I 2/m$ monoclinic space group, while the Co perovskite belongs to $I 4/m$ tetragonal space group. Cell parameters, interatomic distances and tilt angles are all in good agreement with both space groups and ionic radii for Ba²⁺, La³⁺, Mn²⁺, Co²⁺, Ni²⁺ and Sb⁵⁺ ions. Effective presence of Mn²⁺ has been well established by X-ray emission spectroscopy for BaLaMnSbO₆, and there is no evidence of presence of Mn³⁺.

In the compounds, M²⁺ and Sb⁵⁺ ions are distributed over two different crystallographic octahedral sites in a typical rock salt like distribution, with a 6% antisite disorder in Mn and Ni compounds, and only a 1% of disorder for Co material. Rich magnetic ions regions distributed over a bulk characterized by M²⁺–O²⁻–Sb⁵⁺–O²⁻–M²⁺ paths, which can be visualized as nanoclusters, are the responsible by the complex magnetic behavior displayed by BaLaMnSbO₆ double perovskite. BaLaCoSbO₆ and BaLaNiSbO₆ show only the expected 3D-antiferromagnetic behavior, while BaLaMnSbO₆ displays superparamagnetism, which comes from unbalanced antiferromagnetism inside the nanoclusters, at high temperatures, and which is surpassed at low temperatures by the bulk 3D-antiferromagnetic behavior. Powder neutron diffraction data for BaLaMnSbO₆ reveals that at 3 K, long range order antiferromagnetic arrangement of Mn²⁺ spins only on $2d$ octahedral sites is obtained, which is in agreement with the description previously mentioned.

5. Supplementary information

Structural information derived from the crystal structure refinement of BaLaMnSbO₆, BaLaCoSbO₆ and BaLaNiSbO₆ has been deposited at the ICSD Fachinformationszentrum Karlsruhe (FIZ) (E mail: CrysDATA@FIZ.Karlsruhe.DE), with ICSD files numbers 426389, 426390 and 426391 (for BaLaMnSbO₆, at 300, 100 and 3 K, respectively), and 426392 and 426393 (for BaLaCoSbO₆, and BaLaNiSbO₆, respectively, both at 300 K) and 423651(2 K).

Acknowledgements

R.E.C. thanks support from Consejo Nacional de Investigaciones Científicas y Técnicas (CONICET), PIP #11220090100995, the Agencia Nacional de Promoción Científica y Tecnológica (ANPCyT) and the Secretaría de Ciencia y Tecnología de la Universidad Nacional de Córdoba (SECyT-UNC), Project 162/12. J.G. acknowledges support from grants FONCYT PICT 2007-824 and SECyT-UNCuyo 06/C301. We gratefully acknowledge the Institut Laue Langevin (ILL) (Grenoble, France) for access to D2B line, especially to Emmanuelle Sward, and Clemens Ritter for access and time at D1B line.

References

- [1] F.K. Patterson, C.W. Moeller, R. Ward, Magnetic oxides of molybdenum (V) and tungsten (V) with the ordered perovskite structure, *Inorg. Chem.* 2 (1963) 196–198.
- [2] T. Nakagawa, Magnetic and electrical properties of ordered perovskite Sr₂(FeMo)O₆ and its related compounds, *J. Phys. Soc. Jpn.* 24 (1968) 806–811.
- [3] K. Kobayashi, T. Kimura, H. Sawada, K. Terakura, Y. Tokura, Room-temperature magnetoresistance in an oxide material with an ordered double-perovskite structure, *Nature* 395 (1998) 677–680.
- [4] J. Longo, R. Ward, Magnetic compounds of hexavalent rhenium with the perovskite-type structure, *J. Am. Chem. Soc.* 4783 (1961) 2816–2818.
- [5] A.W. Sleight, J.F. Weiher, Magnetic and electrical properties of Ba₂MR₂O₆ ordered perovskites, *J. Phys. Chem. Solids* 33 (1972) 679–687.
- [6] M. Abe, T. Nakagawa, S. Nomura, Magnetic and Mössbauer studies of the ordered perovskites Sr₂Fe_{1+x}Re_{1-x}O₆, *J. Phys. Soc. Jpn.* 35 (1973) 360–365.
- [7] K. Kobayashi, T. Kimura, Y. Tomioka, H. Sawada, K. Terakura, Intergrain tunneling magnetoresistance in polycrystals of the ordered double, *Phys. Rev. B* 59 (1999) 159–162.
- [8] J. Gopalakrishnan, A. Chattopadhyay, S.B. Ogale, T. Venkatesan, R.L. Greene, Metallic and nonmetallic double perovskites: a case study of A₂FeReO₆ (A = Ca, Sr, Ba), *Phys. Rev. B* 62 (2000) 9538–9542.
- [9] D.G. Franco, V.C. Fuytes, M.C. Blanco, M.T. Fernández-Díaz, R.D. Sánchez, R.E. Carbonio, Synthesis, structure and magnetic properties of La₃Co₂SbO₉: a double perovskite with competing antiferromagnetic and ferromagnetic interactions, *J. Solid State Chem.* 194 (2012) 385–391.
- [10] J.-W. Bos, J.P. Attfield, Magnetic frustration in LaCoNbO₆ (A = Ca, Sr, and Ba) double perovskites, *Phys. Rev. B* 70 (2004) 174434.
- [11] M.C. Viola, M.C. Viola, M.J. Martínez-Lope, J.A. Alonso, J.L. Martínez, J.M. De Paoli, S. Pagola, J.C. Pedregosa, M.T. Fernández-Díaz, R.E. Carbonio, Structure and magnetic properties of Sr₂CoWO₆: an ordered double perovskite containing Co²⁺(HS) with unquenched orbital magnetic moment, *Chem. Mater.* 15 (2003) 1655–1663.
- [12] T.K. Mandal, A.M. Abakumov, M.V. Lobanov, M. Croft, V.V. Poltavets, M. Greenblatt, Synthesis, structure, and magnetic properties of SrLaMnSbO₆: a new B-site ordered double perovskite, *Chem. Mater.* 20 (2008) 4653–4660.
- [13] T. Yang, T. Perikias, J. Hadermann, M. Croft, A. Ignatov, M. Greenblatt, B-site ordered perovskite LaSrMnNbO₆: synthesis, structure and antiferromagnetism, *J. Solid State Chem.* 183 (2010) 2689–2694.
- [14] S.S. Pillai, S.N. Jammalamadaka, P.N. Santhosh, Magnetotransport properties of Ba₂MnRuO₆ and LaBaMnRuO₆, *IEEE Trans. Magn.* 43 (2007) 3076–3078.
- [15] H.M. Rietveld, A Profile refinement method for nuclear and magnetic structures, *J. Appl. Crystallogr.* 2 (1969) 65–71.
- [16] J. Rodríguez-Carvajal, Recent advances in magnetic structure determination by neutron powder diffraction, *Physica B* 192 (1993) 55–69.
- [17] G. Tirao, G. Stutz, C. Cusatis, An inelastic X-ray scattering spectrometer at LNL, *J. Synchrotron Radiat.* 11 (2004) 335–342.
- [18] J.A. Bearden, X-ray wavelengths, *Rev. Mod. Phys.* 39 (1967) 78–124.
- [19] A. Faik, J.M. Igartua, M. Gateshki, G.J. Cuello, Crystal structures and phase transitions of Sr₂CrSbO₆, *J. Solid State Chem.* 182 (2009) 1717–1725.
- [20] P.M. Woodward, Octahedral tilting in perovskites. I. Geometrical considerations, *Acta Crystallogr., Sect. B: Struct. Sci.* 53 (1997) 32–43.
- [21] R. Shaheen, J. Bashir, Crystal structure of A₂InSbO₆ (A = Ca, Sr, Ba) ordered double perovskites, *Solid State Sci.* 12 (2010) 605–609.
- [22] T.K. Mandal, V.V. Poltavets, M. Croft, M. Greenblatt, Synthesis, structure and magnetic properties of A₂MnB'O₆ (A = Ca, Sr; B' = Sb, Ta) double perovskites, *J. Solid State Chem.* 181 (2008) 2325–2331.
- [23] A. Faik, D. Orobengoa, E. Iturbe-Zabalzo, J.M. Igartua, A study of the crystal structures and the phase transitions of the ordered double perovskites Sr₂ScSbO₆ and Ca₂ScSbO₆, *J. Solid State Chem.* 192 (2012) 273–283.
- [24] S.A. Larrégola, J.A. Alonso, J.C. Pedregosa, M.J. Martínez-Lope, M. Algueró, V. de la Peña-O'shea, F. Porcher, Francesc Illas, The role of the Pb²⁺ 6s lone pair in the structure of the double perovskite Pb₂ScSbO₆, *Dalton Trans.* (2009) 5453–5459.
- [25] M.C. Viola, J.A. Alonso, J.C. Pedregosa, R.E. Carbonio, Crystal structure and magnetism of the double perovskite Sr₃Fe₂MoO₉: a neutron diffraction study, *Eur. J. Inorg. Chem.* (2005) 1559–1564.
- [26] R.M. Pinacca, M.C. Viola, J.A. Alonso, J.C. Pedregosa, R.E. Carbonio, On the new ferrimagnetic Sr₃Fe₂UO₉ double perovskite with T_C above room temperature: a neutron diffraction study, *J. Mater. Chem.* 9 (2005) 4648–4653.
- [27] M.C. Viola, M.S. Augsburger, R.M. Pinacca, J.C. Pedregosa, R.E. Carbonio, R.C. Mercader, Order–disorder at Fe sites in SrFe_{2/3}B'_{1/3}O₃ (B' = Mo, W, Te, U) tetragonal double perovskites, *J. Solid State Chem.* 175 (2003) 252–257.
- [28] S.S. Raju, B.S. Reddy, M.V.R. Murty, L. Mombasawala, A study of K X-ray hyper-satellites and KMM radiative Auger effect (RAE) of the elements 19 ≤ Z ≤ 25 by photon excitation, *X-Ray Spectrom.* 36 (2007) 35–41.
- [29] S.P. Limandri, A.C. Carreras, R.D. Bonetto, J.C. Trincavelli, Kβ satellite and forbidden transitions in elements with 12 < Z < 30 induced by electron impact, *Phys. Rev. A* 81 (2010) 012504.
- [30] J.A. Bearden, A.F. Burr, Reevaluation of X-ray atomic energy levels, *Rev. Mod. Phys.* 39 (1967) 125–142.
- [31] P. Glaztel, U. Bergmann, High resolution 1s core hole X-ray spectroscopy in 3d transition metal complexes – electronic and structural information, *Coord. Chem. Rev.* 249 (2005) 65–95.
- [32] S.D. Gamblin, D.S. Urch, Metal Kβ X-ray emission spectra of first row transition metal compounds, *J. Electron Spectrosc. Relat. Phenom.* 113 (2001) 179–192.
- [33] K. Tsutsumi, H. Nakamori, K. Ichikawa, X-ray Mn Kβ emission spectra of manganese oxides and manganates, *Phys. Rev. B* 13 (1976) 929–933.
- [34] S. Limandri, S. Ceppi, G. Tirao, G. Stutz, C.G. Sánchez, J.A. Riveros, High resolution study of Kβ' and Kβ1,3 X-ray emission lines from Mn-compounds, *Chem. Phys.* 367 (2010) 93–98.
- [35] A. Meisel, G. Leonhardt, R. Szargan (Eds.), *X-Ray Spectra and Chemical Binding*, vol. 37, Springer-Verlag, New York, 1989, p. 458.
- [36] B. M Nagabhushana, G.T. Chandrappa, R.P. Sreekanth Chakradhar, K.P. Ramesh, C. Shivakumara, Synthesis, structural and transport properties of nanocrystalline La_{1-x}Ba_xMnO₃ (0.0 ≤ x ≤ 0.3) powders, *Solid State Commun.* 136 (2005) 427–432.
- [37] D.G. Franco, R.E. Carbonio, G. Nieva, Magnetic properties of the double perovskites LaPbMSbO₆ (M = Mn Co, and Ni), *IEEE Trans. Magn.* 49 (2013) 4594–4597.
- [38] J.E. Greedan, Geometrically frustrated magnetic materials, *J. Mater. Chem.* 11 (2001) 37–53.
- [39] T. Suominen, J. Raittila, T. Salminen, K. Schlesier, J. Lindén, P. Paturi, Magnetic properties of fine SFMO particles: superparamagnetism, *J. Magn. Magn. Mater.* 309 (2007) 278–284.
- [40] S.K. Srivastava, S. Ravi, Magnetic properties of Nd_{1-x}Ag_xMnO₃ compounds, *J. Phys.: Condens. Matter* 20 (2008) 505212.
- [41] B. Samantaray, S. Ravi, Magnetic properties of Nd_{1-x}K_xMnO₃ compounds, *J. Magn. Magn. Mater.* 321 (2009) 3671–3676.
- [42] S.K. Srivastava, S. Ravi, Magnetic properties of transition metal substituted La_{0.85}Ag_{0.15}Mn_{1-y}M_yO₃ compounds M = Co, Cr and Al, *J. Magn. Magn. Mater.* 321 (2009) 4072–4080.
- [43] B. Samantaray, S. Ravi, Ferromagnetic and charge-ordered phases in (Nd, Na)–Mn–O compounds, *J. Supercond. Novel Magn.* 24 (2010) 809–814.
- [44] B. Samantaray, S. Ravi, A. Perumal, I. Dhiman, A. Das, Neutron powder diffraction studies and magnetic properties in Nd_{1-x}K_xMnO₃ (x = 0.15 and 0.20) compounds, *J. Appl. Phys.* 109 (2011) 07E150.